www.czasopisma.pan.pl PAN www.journals.pan.pl
Opto-Electronics Review 27 (2019) 105–112

Contents lists available at ScienceDirect

Opto-Electronics Review

journal homepage: http://www.journals.elsevier.com/opto-electronics review

Full Length Article

Characterization techniques of sandwich-type TiO_2/QD composites for low-cost quantum dots' solar cell

P. Kwaśnicki [a,b], M. Jarzębski [c,*], P. Kardasz [d,e], M. Inglot [f]

[a] Department of Physical Chemistry and Physicochemical Basis of Environmental Engineering, Institute of Environmental Engineering in Stalowa Wola, John Paul II Catholic University of Lublin, ul. Kwiatkowskiego 3A, 37-450 Stalowa Wola, Poland
[b] ML System S.A, Zaczernie 190 G, 36-062 Zaczernie, Poland
[c] Department of Physics and Biophysics, Faculty of Food Science and Nutrition, Poznan University of Life Science, ul. Wojska Polskiego 38/42, 60-637 Poznań, Poland
[d] Foundation for Research and Development, ul. Legnicka 65, 54-206 Wrocław, Poland
[e] Faculty of Automatics and Robotics, Wroclaw School of Information Technology, ul. Wejherowska 28, 54 - 239 Wroclaw, Poland
[f] Department of Physics and Medical Engineering, Rzeszów University of Technology, Al. Powstańców Warszawy 6, 35-959 Rzeszów, Poland

ARTICLE INFO

Article history:
Received 12 December 2018
Received in revised form 19 March 2019
Accepted 20 March 2019
Available online 30 April 2019

Keywords:
TiO_2
Anatase
Quantum dots
Photovoltaics
QDSC

ABSTRACT

There is a high impact of the solar cells on energy manufacturing. For several years the energy efficiency was limited due to base-materials' structural and technological limits. High increase of energy harvesting of solar cells has been observed since the first solar cell based on dye-sensitized colloidal TiO_2 films occurred. One of the most promising solutions are used quantum dots (QD) for light energy conversion. In this paper, we described the use of selected characterization techniques for sandwich-type TiO_2/QD composites for a low-cost quantum dots' solar cell in the point of view of mass manufacturer of solar cells and research and development laboratory. Moreover, the increasing role of Raman spectroscopy and mapping for the TiO_2/QD was presented and compared with other necessity techniques for solar cell investigations such as ellipsometry, atomic force microscopy (AFM), and secondary ion mass spectrometry (SIMS).

1. Introduction

High increase of electrical devices on daily use brings high demand of the electricity production. On the other side, traditional power resources strongly decrease. One of the solutions is sunlight harvesting by solar cells. For several years, the common use of solar cells was limited by high costs and low efficiency. In 1991 O'Regan and Michael Grätzel proposed a low-cost, high-efficiency solar cell based on dye-sensitized colloidal TiO_2 films [1] which are now called dye-sensitized solar cells (DSSC).

DSSC cells consist of sensitizing dye, transparent conducting substrates (F-doped tin oxide), nanometer-sized TiO_2 [2] film, iodide electrolyte, and counter electrode (Pt or carbon). When a dye molecule absorbs light, it excites electrons on the highest occupied molecular orbital to the lowest unoccupied molecular orbital. The excited dye molecule injects an electron into the conducting band of the TiO_2 film. The oxidized dye is restored by electron donation from the reducing ions in the electrolyte, usually being an organic solvent containing a redox system. The donated electron is in turn regenerated by the reduction of conjugated ions in the electrolytes. The circuit is competed by electron migration through an external load [3]. In this kind of a solar cell, TiO_2 plays a very essential role.

It is evident that the specific structure of the TiO_2 layer may have an influence on increasing the efficiency of DSSCs. Therefore, many specific TiO_2 nanostructures were studied theoretically [4] and practically [5–7], to name just a few like nanofibre–nanoparticle composite electrodes [8], nanowire-based composite electrodes [9,10], nanofibre based electrodes [11], nanorods – nanoparticle-based composite electrodes [12], nanoparticle– nanowire composite electrodes [13], TiO_2 nanowires, and highly ordered TiO_2 nanotube arrays [14]. The dye-sensitized nanocrystalline TiO_2 film plays an important role in a DSSC. There are many methods for preparing TiO_2 thin films on the conductive side of fluorine-doped tin oxide (FTO) glasses: sol-gel method [13], physical vapor deposition (PVD) [15], liquid phase deposition [16], a spin-coating method [17], and screen printing technology [18,19]. Compared with other methods, the film thickness can be easily controlled in screen printing by the selection of paste composition, screen mesh size and printing times.

The most intensive progress with DSSC is observed in recent years, while quantum dots (QD) are used for light energy conversion

* Corresponding author.
E-mail addresses: pawel.kwasnicki@mlsystem.pl (P. Kwaśnicki), maciej.jarzebski@o2.pl, maciej.jarzebski@up.poznan.pl (M. Jarzębski), p.kardasz@kbri.pl (P. Kardasz), ming@prz.edu.pl (M. Inglot).

https://doi.org/10.1016/j.opelre.2019.03.001
1230-3402/

[20,21]. The systems named quantum dots' solar cell (QDSC) brings new opportunities according to QD size-tunable optical properties [22,23]. Raman spectrometry is useful to verify the presence, distribution or structure [24] of additives of nanocomponents, such as graphene oxide [25,26], fluorite structure–metal-dioxide of CeO_2 [27] and SnO_2 [28] particles or modified CdS:Zn quantum dots [29]. Raman techniques are adequate for surface mapping of solar cells to evaluate the homogeneity of the structure [30].

From the mass manufacturer's point of view, the relation between manufacturing costs and profits plays a key role. The second main factor is easy access for the main suppliers of the critical product components and their ability to supply the same quality products. It is especially important when new nanomaterials, such as quantum dots are used. For that reason, in this paper, we decided to present the investigations of QDSC photovoltaic system which is based on quite easy access commercially available materials, such as titania paste and Zn-Cu-In-S/ZnS quantum dots. Moreover, we have described the results obtained from the most important characterization techniques used by research and development department of the new designed QDSC. The presented Raman spectroscopy, microscopic, secondary ion mass spectrometry, and ellipsometry techniques bring a quick answer to the main question: is the proposed system worth to deeper investigations and could it be applied for mass production. Furthermore, our results show that the Raman techniques might play a key role in rapid measurements in innovative research and development centers.

2. Materials and methods

2.1. Materials

Titanium dioxide layer was made using Dyesol's 18NR-T Transparent Titania Paste. The crystal structure was 99% of anatase with the particles size of approximately 20 nm in diameter. The viscosity of the paste is between 40,000–55,000 mPa s. Dyesol's 18NR-T Transparent Titania Paste has highly dispersed and stable anatase nanoparticles and is optimized for screen printing using a synthetic 43 T mesh screen.

Commercially available Zn-Cu-In-S/ZnS quantum dots were purchased from PlasmaChem Gmbh. The used QD were cadmium free, coated with hydrophobic organic ligands soluble in toluene. The emission peak width full with of half maximum (FWHM) was ca. 100 nm and large Stokes shift ca. 120 nm. Typical quantum yield for QD was 40–70 % with diameter 4–5 nm.

2.2. Samples preparation

In this study, triple layer sandwich-type samples' TiO_2/QD composites were prepared during the three-step procedure (see Fig. 1). First, as a groundwork a 1 mm thick float glass covered by transparent conductive oxide (TCO) layer, in this case, CVD deposited FTO was used. In the second step, on the top of the FTO layer, the TiO_2 layer was made using a screen printing technique. Finally above the TiO_2, quantum dots (QDs) were deposited using the deposition technique: n-areo.

2.3. Methods

The surface investigations were performed using high-resolution scanning electron (SEM), atomic force microscopy (AFM), and secondary ion mass spectroscopy (SIMS). Optical measurements were done using Ellipsometry and Raman spectroscopy to investigate thickness, optical and electrical parameters, as well as phase identification.

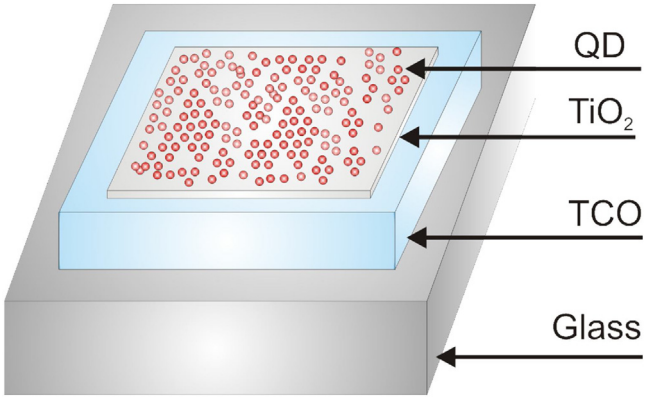

Fig. 1. Schematic representation of the structure of QDSC.

Scanning electron microscope (SEM) FEI Verios for sample imaging was used. The SEM was equipped with in-column backscatter detector (ICD) which provides no loss material contrast, mirror detector (MD) which provides low loss material contrast, ICD detector enabling low kV resolution at high immersion ratios, and energy dispersive spectroscopy (EDS) detectors. The images were registered at the accelerating voltage varied from 1 to 2 keV and working distance between 2 and 4 mm.

AFM measurements were done using AFM Agilent 750 system which provides spatial information parallel and perpendicular to the surface. In addition to topographic high-resolution information, local material properties such as adhesion and stiffness can be investigated by analyzing tip-sample interaction forces. System equipped with five 24-bit scan drives for high resolution and accuracy, two 24-bit output channels for controlling imaging parameters. The scanning range is formed of 9 μm × 9 μm up to 90 μm × 90 μm, Z range of 8 μm and the vertical noise of 0.5 Å RMS. Measurements were done in room temperature in a tipping mode set-up.

SIMS (secondary ion mass spectrometry) investigations were made using TOF SIMS system from ION-TOF equipped with a reflectron TOF analyser giving high secondary ion transmission with high mass resolution and sample chamber with a 5-axis manipulator (x, y, z, rotation and tilt) for flexible navigation, a fast entry load-lock, charge compensation for the analysis of insulators.

RAMAN - for the TiO_2/QDs composites structure investigations, Raman spectra were obtained by LabRam HR system from Horiba. A Helium-Neon (HeNe) laser with an excitation wavelength $\lambda = 632.8$ nm of the internal 17 mW was used. The system was equipped with a confocal microscope coupled to an 800 mm focal length achromatic spectrograph and a two-dimensional multichannel CCD camera. Measurements were done in room temperature.

Ellipsometry - the electric and optical parameters, as well as the thickness of the layer were studied using the SE-2000 modular optical platform including a spectroscopic ellipsometer with rotating compensator optics. Non-contact and non-destructive optical measurements on substrates, single layer and multi-layer samples to obtain individual thin film thickness and optical properties were done. Measurements were performed in room temperature in a spectral range of 250–1100 nm and an angle fixed at 70°.

3. Results and discussion

3.1. Surface and size investigations

The presented layer was made using screen printing technology and the thickness of the layer was estimated to be in the range of 5 μm according to the deposition process. Substrate for

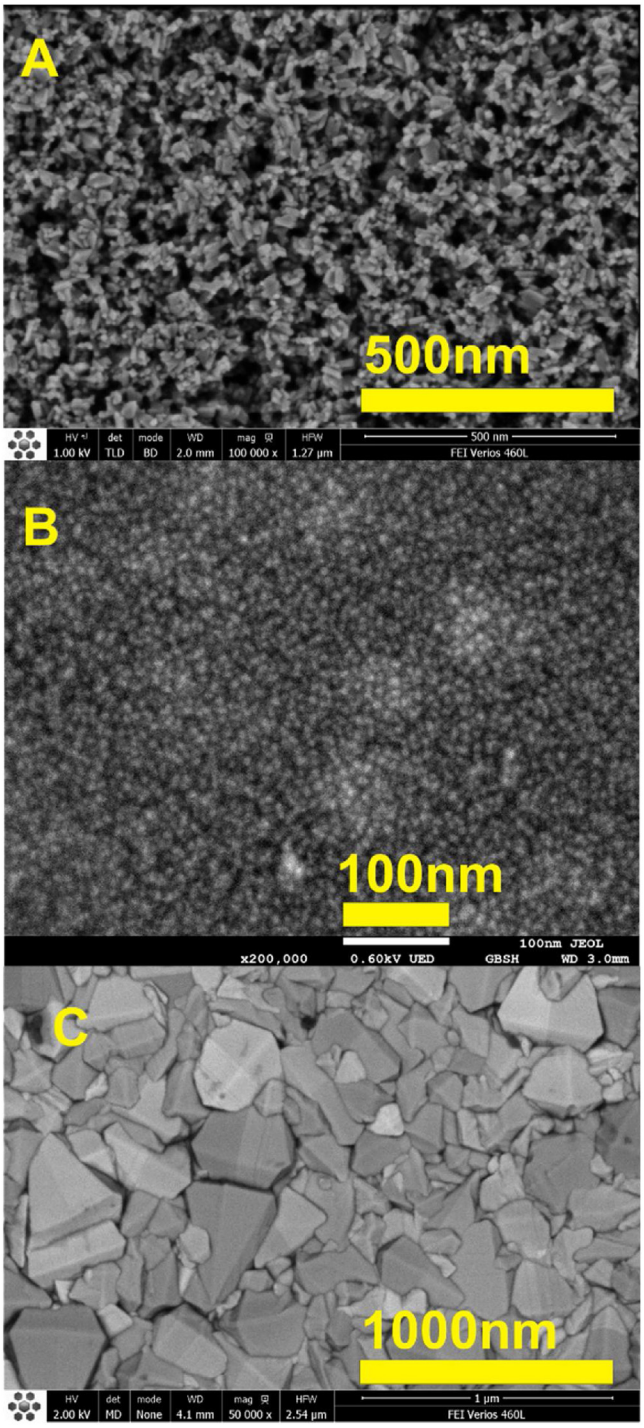

Fig. 2. SEM images: A. surface topography of TiO_2 taken using SE detector with a magnification of 100kx, B. surface topography of TiO_2 layer with QDs on the top took using SE detector with a magnification of 200kx, C. surface topography of TCO took using SE detector with a magnification of 50kx.

the TiO_2 deposition was glass coated with FTO thin layer with a thickness of around 600 nm, what is a widely used architecture for the building of a DSSC or QDs solar cell. A typical picture of TiO_2 and TCO topography with different magnification is shown in Figs. 2A, 2B, 2C. High magnification and high-resolution images show a mesoporous structure of the TiO_2 layer (Figs. 3A, 3B). This kind of structure is favorable for both DSSC and QDSC regarding the fact that the absorber is either liquid in case of DSSC or small particles in case of QDSC. The accelerating voltage was fixed on 2 keV for TCO and TiO_2, and 0.8 keV for QDs layer, the working distance between 4.1 and 2 mm. Since the TiO_2 layer is a low conducting material a charge accumulation effect was observed, in order to overcome the effect on the imaging a drift correction function was used.

One can clearly see the typical structure of the transparent conductive layer (Fig. 2C) composed with crystallites closely linked. Since TCO is a conductive layer SEM investigation of topography is easy and one can use even higher accelerating voltage. No inhomogeneity in terms of chemical compounds, in this case, was observed done with higher magnification clearly illustrates the mesoporous structure of TiO_2 (Figs. 3A and 3B). This structure and electrical properties of TiO_2 makes the measurements difficult and complicates the investigation of nanoparticles (see Fig. 3C).

Nonetheless, since TiO_2 is widely used the material in photovoltaic as a photoanode, finding a way of characterization of QDs on TiO_2 is critical. One of the obstacles is the charge accumulation effect which hardly enables observation of nanostructures such as quantum dots. In order to overcome this problem it is necessary to decrease both the accelerating voltage and the current intensity, as well as use the drift correction feature. Due to these features, we could obtain a clear good quality image of the material. The size of the TiO_2 crystallites was found to be in the range between around 7 and 20 nm. This difference is a result of used deposition technique namely screen printing. Quantum dots are visible on the top as a non-continuous layer. The diameter of the QDs was found to be in a range of about 6 nm.

AFM measurements done on the samples without and with QDs shows a slight difference. Clear TiO_2 layer measured by AFM shows a mesoporous structure (see Fig. 4A). The crystallites are sharp edges and the Z contrast ranges up to around 115 nm. One can notice random distribution of the material with rough surface topography.

A sample of TiO_2 after deposition of QDs differs from the clear TiO_2 layer (see Fig. 4B). No clear images of QDs are visible nonetheless now sharp edges of TiO_2 are the more rounded shape. This is attributed to the presence of small in diameter quantum dots which possible fulfill the holes between the substrate material and stick to the edges. One can also notice that the roughness of the surface decreases for the samples with QDs compared to the clear TiO_2 layer.

Measurements show that the size of the crystallites ranges from tens of nanometres up to few hundreds of nanometres. This could be related to the presence of QDs which linked to the TiO_2 crystallites form bigger structures. Even though one can assume presence of QDs because of the difference in topography, AFM does not allow to estimate the size of quantum dots on a highly rough substrate such as TiO_2. Possible way to measure directly the diameter and investigate the shape of the QDs is to place them on flat surface, e.g.: silicon wafer, in this way one should easily obtain the requested information.

3.2. *Structure analysis*

SIMS measurements were done on the samples without quantum dots as a reference sample (Fig. 5A) and on the samples with the layer of QDs (Fig. 5B). For both measurements, Cs^+ as a primary ion beam with an energy of 10 keV was used. The crater size is 5×5 µm. Figures 5A and 5B show the counts *vs.* erosion time for all acquired signals. Erosion time is directly proportional to the depth of the crater, nonetheless, no profile calibration was done to estimate the exact depth. One can only say that shorter time corresponds to the upper part of the sample.

For both profiles the presence of the Ti, C, Na, is easily noticeable. The main difference one can see between profiles A and B is a presence of metals such as Zn, Cu, In which are the compounds of the quantum dots. The occurrence of these elements clearly indicates

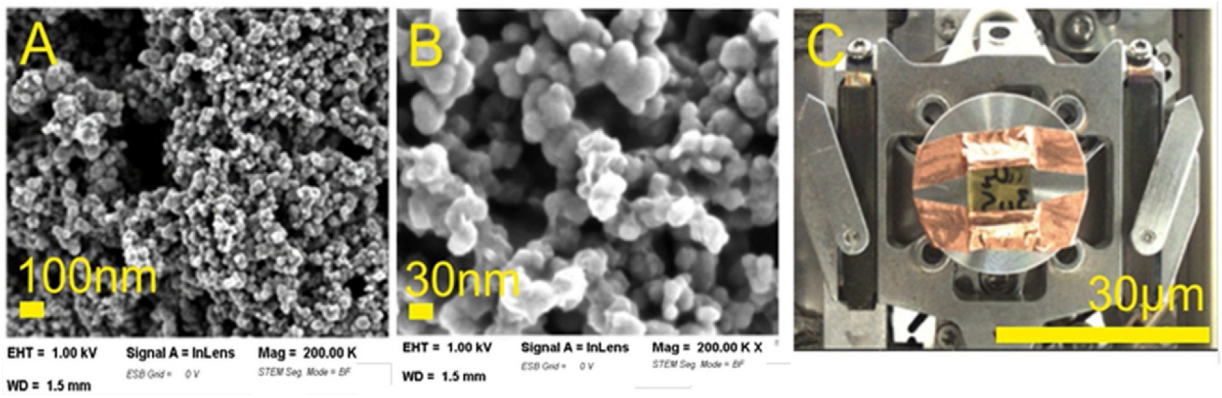

Fig. 3. SEM images of mesoporous structure of TiO_2,: A., B., C. sample in the measuring chamber.

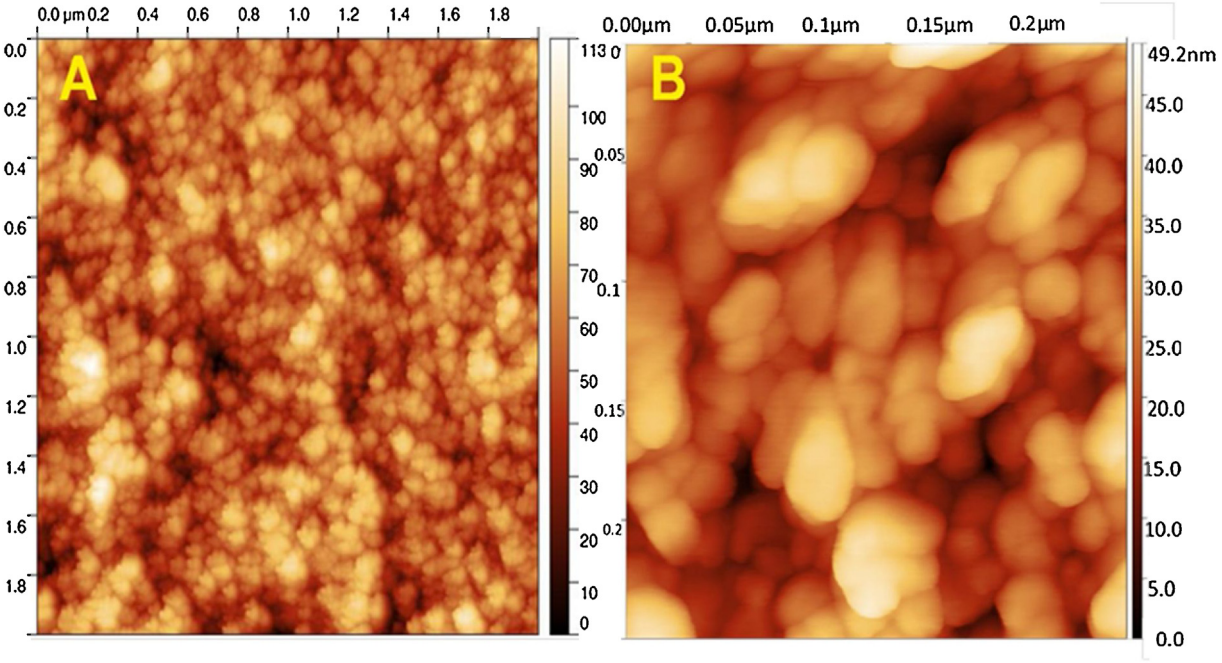

Fig. 4. AFM image of the surface taken from the sample: A. without QDs, B. containing QDs.

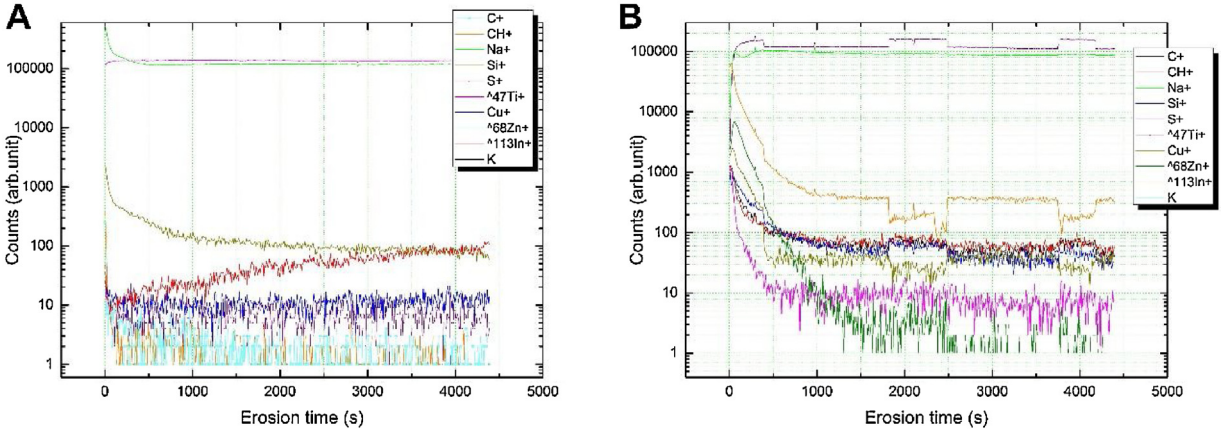

Fig. 5. SIMS profiles for two investigated samples: A. TiO_2 layer, B. TiO_2 layer with QDs on the top.

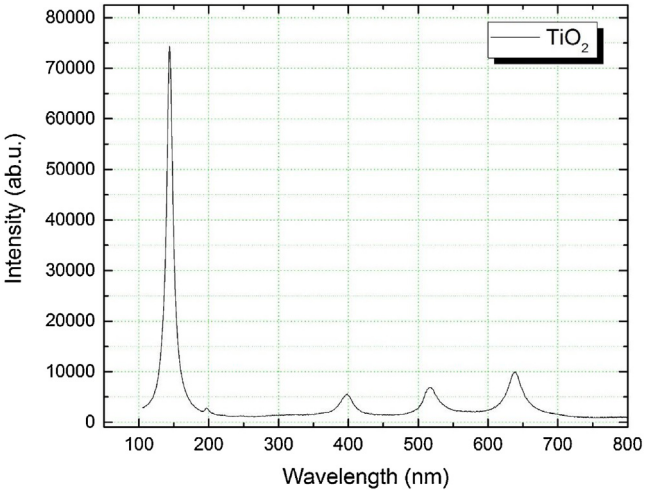

Fig. 6. Raman spectra of TiO_2 taken using 6328 nm wavelength as the excitation source.

that the quantum dots are present on the surface of the sample. We can see that the presence of these elements is only noticeable in the first 800 s of the erosion, so we can conclude that quantum dots are present only on the top of the TiO_2 and do not penetrate the mesoporous layer deeply.

A typical structure of TiO_2 is shown in Fig. 6. Clear peaks allow to easily identify the polytype, in this case, is anatase. No Inclusion of other polytypes or significant defects is noticeable. TiO_2 anatase is tetragonal and belongs to the space group $D^{19h}{}_{14h}$ (I4amid). The primitive unit cell contains two TiO_2 chemical units. According to the factor group analysis, the 15 optical modes have the irreducible representation $1A_{1g}$, $1A_{2u}$, $2B_{1g}$, $1B_{2u}$, 3 Eg, $2E_u$. The modes A_{1g}, B_{1g}, and E_g are Raman active and the modes $1A_{2u}$ and E_u, are infrared active. The B_{2u} mode is inactive both in the Raman and infrared spectra. Raman modes seen in Fig. 4 are assigned to the Raman spectra of the anatase single crystal [10]: ~144 cm^{-1} (E_g), 197 cm^{-1} (E_g), 399 cm^{-1}, (B_{1g}), 513 cm^{-1} (A_{1g}), 519 cm^{-1} (B_{1g}) and 639 cm^{-1} (E_g).

Next Raman measurements were done on the samples containing QDs on the top. Since the layer of QDs is thin and not homogenous to obtain any trace of the nanoparticles a larger area of the surface was analyzed using mapping mode (see Fig. 7). Again clear signature of TiO_2 is noticed, as well as a large peak in the range of 330 cm^{-1}. Since in case of anatase we do not expect to see any peak between 197 cm^{-1} and 399 cm^{-1} this peak was assigned to the presence of quantum dots. The peak appears only for samples containing QDs and on the area where QDs are expected to be (the brighter area on the sample).

3.3. Ellipsometry

Thickness, since it one of the key parameters was estimated using ellipsometry technique. To estimate the thickness of the TiO_2 layer, first of all, we measured TCO layer on glass since ellipsometric measurements done on a complex structure could be difficult to analyze. The TCO sample was modeled using an already very complex model, describing the single films using 4 layers in total. Tables 1 and 2 show a schematic representation of the layers used for the modeling. The reason is a graded refractive index of the TOC film. Measurements results are shown in Figs. 8 and 9.

The dispersion of the TCO film was described using a spectral combination of a Tauc-Lorentz oscillator mode and Drude absorption. The optical model includes a total number of three individual TCO sublayers, as well as a roughness on top, to obtain a fairly good fitting. The real structure of the TCO films seems to be even more complex. The total TCO (3 * TCO + roughness) film thickness was determined to d = 816 nm.

Next, the stuck of TiO_2 on TCO was measured. For this, the same model of TCO was used but this time the TiO_2 layer on the top was added as shown in Figs. 10 and 11. The TiO2 / TCO / glass shows high-

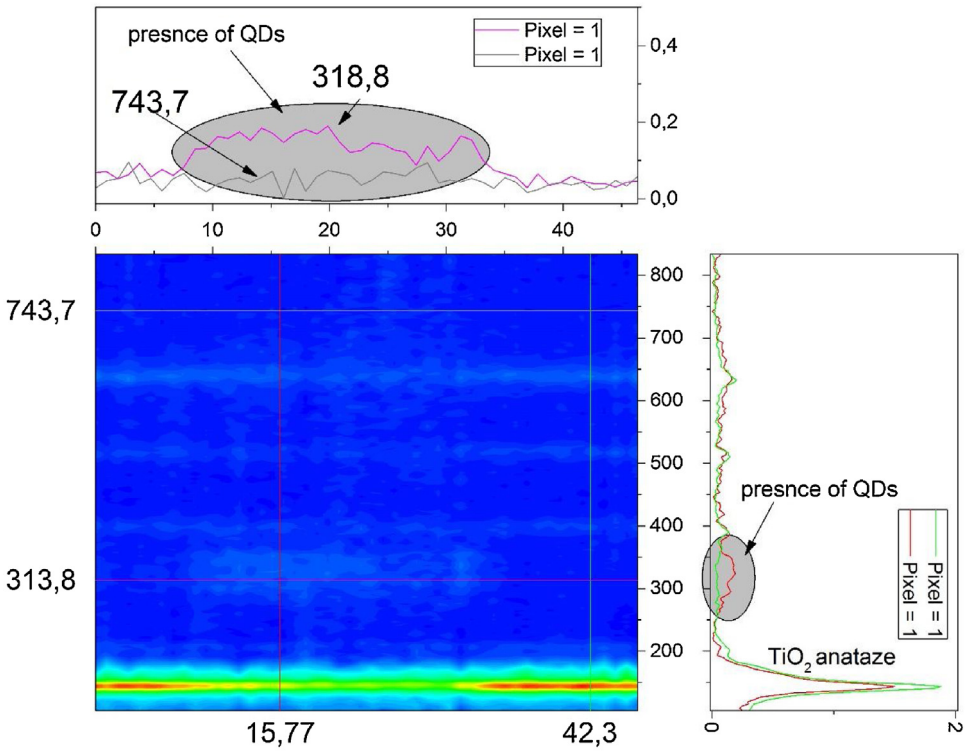

Fig. 7. Raman mapping on the TiO_2 sample with quantum dots on the top.

Table 1
Schematic representation of the TCO layers used for the modeling.

Layer	Thickness(nm)	Layer type	n/k (λ = 632.8 nm)
Air	–	NK layer	n = 1.0000
Roughness Air/x0	32.30	Effective medium and interface	n = 1.3648 k = 0.00107
TCO – SC 1	37.73	Spectral combination layer	n = 1.7637 k = 0.00231
TCO – SC 2	570.22	Spectral combination layer	n = 1.8830 k = 0.04593
TCO – SC 3	176.16	Spectral combination layer	n = 1.8155 k = 0.26722
Glass	–	Cauchy layer	n = 1.5214

Table 2
Schematic representation of the TCO + TiO2 layers used for the modeling.

Layer	Thickness(nm)	Layer type	n/k (λ = 632.8 nm)
Air	–	NK layer	n = 1.0000
Roughness 2	32.00	Effective medium and interface	n = 1.6671
TiO_2	5000.00	Tauc-Lorentz layer	n = 2.4256
Roughness 1	32.30	Effective medium and interface	n = 2.0860 k = 0.00122
TCO – SC 1	37.73	Spectral combination layer	n = 1.7637 k = 0.00231
TCO – SC 2	570.22	Spectral combination layer	n = 1.8830 k = 0.04593
TCO – SC 3	176.16	Spectral combination layer	n = 1.8155 k = 0.26722
Glass	–	Cauchy layer	n = 1.5214

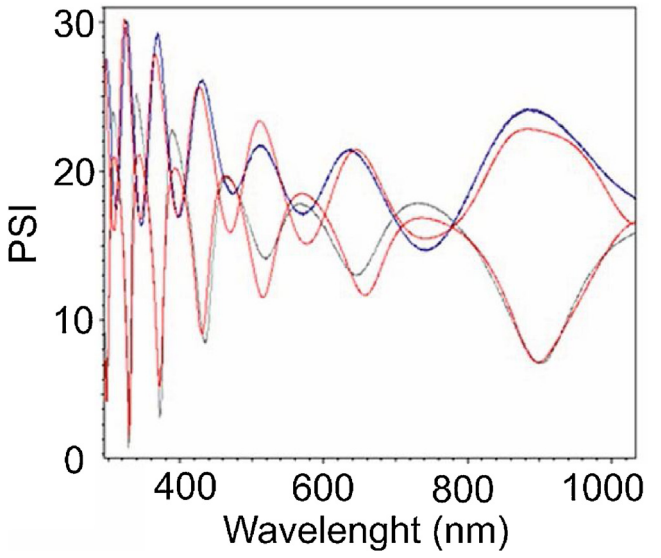

Fig. 8. Schematic optical model of the TCO layers along with measured and modeled (red) PSI.

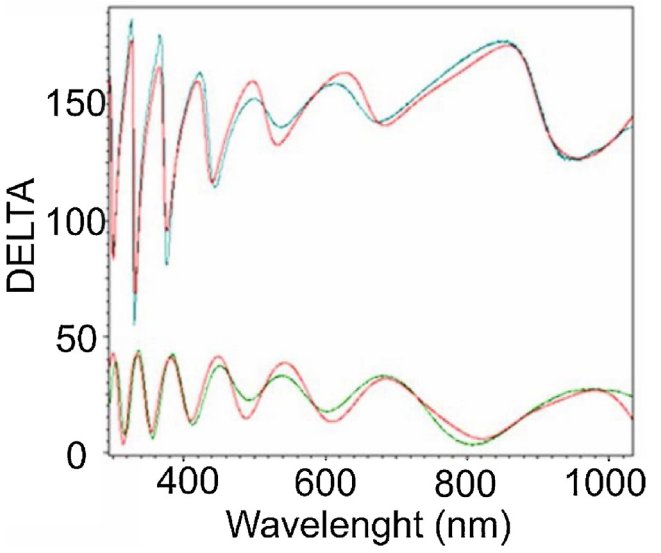

Fig. 9. Schematic optical model of the TCO layers along with measured and modeled DELTA spectra at an AOI of 50° and 70°.

frequency interference fringes due to the high TiO_2 film thickness. These fringes are extremely damped. The reason can be a high film thickness inhomogeneity.

When TiO_2 of 5 μm film thickness is introduced into the model, a huge mismatch between measurement and model is observed. The damping is too strong to find a reasonable model for that. We conclude that the ellipsometry is not an optimal technique to estimate the thickness of the TiO_2 layer made by screen printing. Due to the issues in the spectral range where the TCO and TiO_2 are transparent (VIS), the modeling of the QD was tried in the UV spectral range instead. There, TiO_2 is opaque and becomes the substrate material in the optical model, underlying layers become invisible, and the model becomes simpler. However, a reasonable model was not found. The reason might be a strong roughness on top if the TiO_2 film. Furthermore, the differences in the TiO_2 film might be stronger than the influence of the QD layer making it difficult to find an optical model for the QD layer.

3.4. Photoluminescence

Photoluminescence measurements were done in room temperature using a 380 nm wavelength as an excitation source. The signal was acquired by CCD camera. Results of measurements done on the TiO_2 layer (blue line) and stack TiO_2 + QDs (red line) are shown in Fig. 12. For TiO_2 layer just a typical signature of this material is visible. We do not observe any trace of other elements. Three peaks are clearly visible. The peak at 404 nm is attributed to the free exciton emission near the fundamental band edge. The excitonic peak at 419 nm is attributed to the recombination of self-trapped excitons in anatase TiO_2. Peaks in the range of 500–700 nm are identified as phonon replicas in anatase TiO_2 and arise from the excitonic $e^- - h^+$ recombination via oxygen vacancies. Since the measurements were done in room temperature and low spectral resolution, it's not possible to well resolve all peaks of excitonic and band-band transitions.

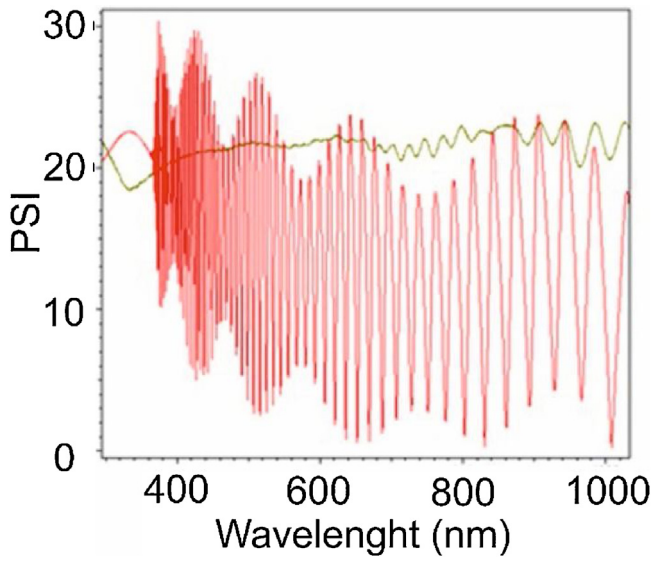

Fig. 10. Schematic optical model of the TCO + TiO_2 layers along with measured and modeled (red) PSI.

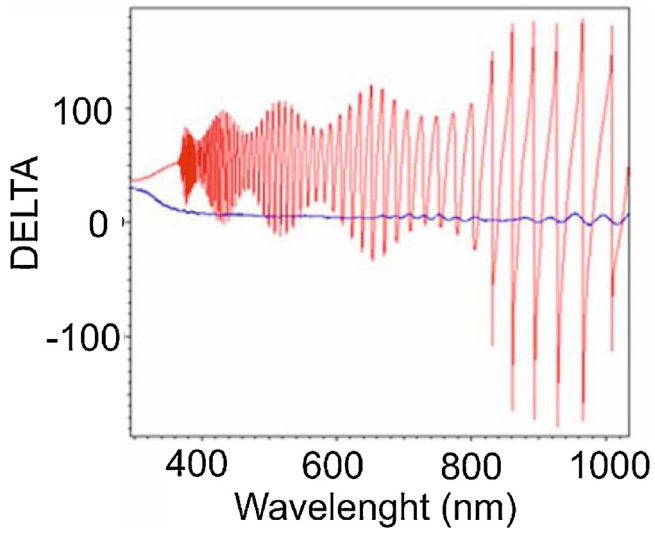

Fig. 11. Schematic optical model of the TCO + TiO_2 layers along with measured and modeled DELTA spectra at an AOI of 50° and 70°.

Red line corresponds to the samples containing quantum dots on the top. An intense peak appears at 521 nm. Since we did not observe it for clear TiO_2 layer, we conclude then this peak comes from the presence of quantum dots. In addition in case of anatase or even rutile typical PL bands appear as a peak in the range of 400–490 nm arising from an excitonic $e^- - h^+$recombination via oxygen vacancies, so we do not expect to see any features at 521 nm. This clearly points at the presence of QDs.

4. Conclusions

In this work, we present a complex analysis of TiO_2 anatase layer and TiO_2 + QDs. A wide range of techniques was used in order to obtain detailed information about the measured layer. It was shown that complementary study is necessary for clear and unquestionable identification of nanoparticles on the mesoporous structure such as TiO_2. We showed that both structural and spectral analysis are equally useful regarding the required information. All technique is considered being complimentary and can provide additional information concerning distribution, size, optical and electrical parameters for substrate and quantum dots.

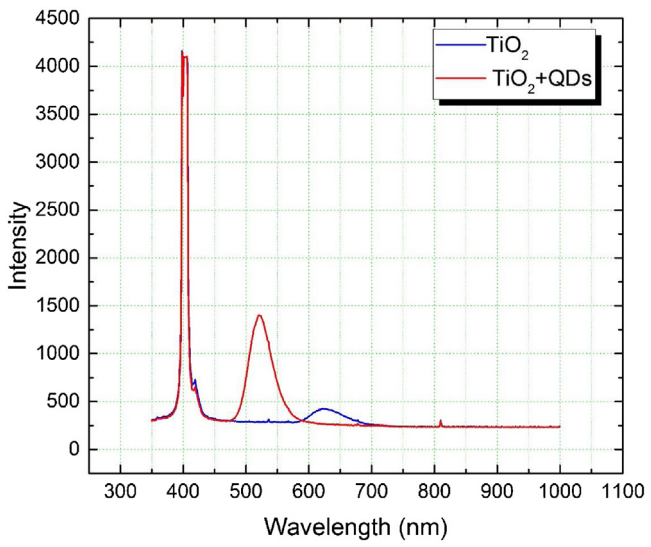

Fig. 12. Photoluminescence spectra taken on samples TiO_2 (blue line) and samples with QDs (red line).

Conflict of interest

The authors declare that there is no conflict of interest regarding the publication of this paper.

Acknowledgements

This work was supported by the National Centre for Research and Development under the project No. POIR.01.01.01.00-0598/15-00 and UDA-RPPK.01.03.00-18-025/13-00. This work was partially supported by ML System S.A, Zaczernie 190G, 36-062 Zaczernie, Poland.

References

[1] B. O'Regan, M. Grätzel, A low-cost, high-efficiency solar cell based on dye-sensitized colloidal TiO_2 films, Nature 353 (1991) 737–740, http://dx.doi.org/10.1038/353737a0.
[2] M.A.K.L. Dissanayakea, DH.K.D.W.M.N. Divarathna, C.B. Dissanayake, G.K.R. Senadeera, P.M.P.C. Ekanayake, C.A. Thotawattage, An innovative TiO_2 nanoparticle/nanofibre/nanoparticle, three layer composite photoanode for efficiency enhancement in dye-sensitized solar cells, J. Photochem. Photobiol. A 322–323 (2016) 110–118, http://dx.doi.org/10.1016/j.jphotochem.2016.02.017.
[3] M. Grätzel, Solar energy conversion by dye-sensitized photovoltaic cells, Inorg. Chem. 44 (20) (2005) 6841–6851, http://dx.doi.org/10.1021/ic0508371.
[4] F.E. Gálvez, E. Kemppainen, H. Míguez, J. Halme, Effect of diffuse light scattering designs on the efficiency of dye solar cells: an integral optical and electrical description, J. Phys. Chem. C 116 (21) (2012) 11426–11433, http://dx.doi.org/10.1021/jp2092708.
[5] A. Tereshchenko, V. Smyntyna, A. Ramanavicius, Interaction mechanism between TiO_2 nanostructures and bovine leukemia virus proteins in photoluminescence-based immunosensors, RSC Adv. 8 (2018) 37740–37748, http://dx.doi.org/10.1039/c8ra07347c.
[6] R. Viter, A. Tereshchenko, V. Smyntyna, J. Ogorodniichuk, N. Starodub, R. Yakimova, V. Khranovskyy, A. Ramanavicius, Toward development of optical biosensors based on photoluminescence of TiO_2 nanoparticles for the detection of Salmonella, Sens. Actuators B-Chem. 252 (2017) 95–102, http://dx.doi.org/10.1016/j.snb.2017.05.139.
[7] M. Dominik, E. Roźniecka, Ł. Wachnicki, J. Niedziółka-Jönsson, M. Godlewski, W.J. Bock, M. Śmietana, Biofunctionalization effectiveness of titanium oxide thin films obtained with physical and chemical vapour deposition methods for optical label-free biosensing applications, Proc. Tech. 27 (2017) 232–233, http://dx.doi.org/10.1016/j.protcy.2017.04.098.
[8] P. Joshi, L. Zhang, D. Davoux, Z. Zhu, D. Galipeau, H. Fong, Q. Qiao, Composite of TiO_2 nanofibers and nanoparticles for dye-sensitized solar cells with

significantly improved efficiency, Energy Environ. Sci. 3 (2010) 1507–1510, http://dx.doi.org/10.1039/C0EE00068J.
[9] K. Asagoe, Y. Suzuki, S. Ngamsinlapasathian, S. Yoshikawa, TiO_2-anatase nanowire dispersed composite electrode for dye-sensitized solar cells, J. Phys. Conf. Ser. 61 (2007) 1112–1116, http://dx.doi.org/10.1088/1742-6596/61/1/220.
[10] J.B. Baxter, E.S. Aydil, Nanowire-based dye-sensitized solar cells, Appl. Phys. Lett. 86 (2005) 053114, http://dx.doi.org/10.1063/1.1861510.
[11] D. Sabba, S. Agarwala, S.S. Pramana, S. Mhaisalkar, A maskless synthesis of TiO_2-nanofiber-based hierarchical structures for solid-state dye-sensitized solar cells with improved performance, Nanoscale Res. Lett. 9 (2014) 14–23, http://dx.doi.org/10.1186/1556-276X-9-14.
[12] S. Pavasupree, S. Ngamsinlapasathian, M. Nakajima, Y. Suzuki, S. Yoshikawa, Synthesis, characterization, photocatalytic activity and dye-sensitized solar cell performance of nanorods/nanoparticles TiO_2 with mesoporous structure, J. Photochem. Photobiol. A 184 (2006) 163–169, http://dx.doi.org/10.1016/j.jphotochem.2006.04.010.
[13] B. Tan, Y. Wu, Dye-sensitized solar cells based on anatase TiO_2 nanoparticle /nanowire composites, J. Phys. Chem. B 110 (32) (2006) 15932–15938, http://dx.doi.org/10.1021/jp063972n.
[14] G.K. Mor, K. Shankar, M. Paulose, O.K. Varghese, C.A. Grimes, Use of highly-ordered TiO2 nanotube arrays in dye-sensitized solar cells, Nano Lett. 6 (2) (2006) 215–218, http://dx.doi.org/10.1021/nl052099j.
[15] M.C. Kao, H.Z. Chen, S.L. Young, C.Y. Kung, C.C. Lin, The effects of the thickness of TiO_2 films on the performance of dye-sensitized solar cells, Thin Solid Films 517 (2009) 5096–5099, http://dx.doi.org/10.1016/j.tsf.2009.03.102.
[16] S.C. Yang, D.J. Yang, J. Kim, J.M. Hong, H.G. Kim, I.D. Kim, H. Lee, Hollow TiO_2 hemispheres obtained by colloidal templating for application in dye-sensitized solar cells, Adv. Mater. 20 (2008) 1059–1064, http://dx.doi.org/10.1002/adma.200701808.
[17] J.G. Lee, J.H. Cheon, H.S. Yang, D.K. Lee, J.H. Kim, Enhancement of photovoltaic performance in dye-sensitized solar cells with the spin-coated TiO_2 blocking layer, J. Nanosci. Nanotechnol. 12 (2012) 6026–6030, http://dx.doi.org/10.1166/jnn.2012.6410.
[18] T. Charinpanitkul, P. Lorturn, W. Ratismith, N. Viriya-empikul, G. Tumcharern, J. Wilcox, Hydrothermal synthesis of titanate nanoparticle/carbon nanotube hybridized material for dye sensitized solar cell application, Mater. Res. Bull. 46 (2011) 1604–1609, http://dx.doi.org/10.1016/j.materresbull.2011.06.012.
[19] S. Ito, P. Chen, P. Comte, M.K. Nazeeruddin, P. Liska, P. Pechy, M. Graetzel, Fabrication of screen-printing pastes from TiO_2 powders for dye-sensitised solar cells, Prog. Photovolt. 15 (2007) 603–612, http://dx.doi.org/10.1002/pip.768.
[20] S. Ruhle, M. Shalom, A. Zaban, Quantum-dot-sensitized solar cells, ChemPhysChem 11 (2010) 2290–2304, http://dx.doi.org/10.1002/cphc.201000069.
[21] Z. Penga, Z. Liu, Y. Liu, J. Chen, C. Li, W. Lia, L. Liao, J. Chen, Improving on the interparticle connection for performance enhancement of flexible quantum dot sensitized solar cells, Mater. Res. Bull. 105 (2018) 91–97, http://dx.doi.org/10.1016/j.materresbull.2018.04.039.
[22] M.B. de la Mora, O. Amelines-Sarria, B.M. Monroy, C.D. Hernández-Pérez, J.E. Lugo, Materials for downconversion in solar cells: perspectives and challenges, Sol. Energy Mater. Sol. C 165 (2017) 59–71, http://dx.doi.org/10.1016/j.solmat.2017.02.016.
[23] A. Majchrowski, G. Lakshminarayana, A.H. Reshak, E. Michalski, M. Olifierczuk, K. Ozga, L. Jaroszewicz, T. Lukasiewicz, M. Szota, M. Nabialek, Laser operated elasto-optical features of La2CaB10O19:Pr3+ polymer nanocomposites, J. Lumin. 132 (10) (2012) 2577–2580, http://dx.doi.org/10.1016/j.jlumin.2012.04.042.
[24] P.R. Ghediya, T.K. Chaudhuri, V. Raj, D. Chugh, K. Vora, L. Li, H.H. Tan, C. Jagadish, Direct-coated Cu2SnS3films from molecular solution inks for solar photovoltaics, Mater. Sci. Semicond. Proc. 88 (2018) 120–126, http://dx.doi.org/10.1016/j.mssp.2018.07.041.
[25] S. Das, K. Sa, I. Alam, P. Mahanandia, Synthesis of CZTS QDs decorated reduced graphene oxide nanocomposite as possible absorber for solar cell, Mater. Lett. 232 (2018) 232–236, http://dx.doi.org/10.1016/j.matlet.2018.08.074.
[26] M.A. Mousa, M. Khairy, H.M. Mohamed, Dye-sensitized solar cells based on an N-doped TiO_2 and TiO_2-graphene composite electrode, J. Electron. Mater. 47 (10) (2018) 6241–6250, http://dx.doi.org/10.1007/s11664-018-6530-0.
[27] B.V. Dias, G.T. Tractz, A. Viomar, G.A.R. Maia, M.T. Da Cunha, P.R.P. Rodrigues, Photoelectrochemical behavior of the cell FTO/TiO_2/CeO_2/ N719 obtained from the Pechini and precipitation of cerium oxide methods, J. Electron. Mater. 47 (9) (2018) 5556–5563, http://dx.doi.org/10.1007/s11664-018-6465-5.
[28] C. Gao, Z. Zhang, X. Li, L. Chen, Y. Wang, Y. He, F. Teng, J. Zhou, W. Han, E. Xie, Synergistic effects in three-dimensional SnO_2/TiO_2/CdS multi-hetero junction n structure for highly efficient photo electrochemical hydrogen production, Energy Mater. Sol. Cells 141 (2015) 101–107, http://dx.doi.org/10.1016/j.solmat.2015.05.026.
[29] M. Banski, M. Chrzanowski, G. Zatryb, J. Misiewicz, A. Podhorodecki, Enhanced photoluminescence stability of CdS nanocrystals through a zinc acetate reagent, RSC Adv. 8 (2018) 25417–25422, http://dx.doi.org/10.1039/c8ra03504k.
[30] S.M.P. Meroni, Y. Mouhamad, F. De Rossi, A. Pockett, J. Baker, R. Escalante, J. Searle, M.J. Carnie, E. Jewell, G. Oskam, T.M. Watson, Homogeneous and highly controlled deposition of low viscosity inks and application on fully printable perovskite solar cells, Sci. Technol. Adv. Mater. 19 (1) (2018) 1–9, http://dx.doi.org/10.1080/14686996.2017.1406777.